Ab-initio calculation of optical properties of monolayer arsenene with substituted atoms

J. D. García-Aguilar

Centro de Estudios Científicos y Tecnológicos No 16, Instituto Politécnico Nacional, Kilómetro 1.500, Actopan-Pachuca, San Agustín Tlaxiaca, Hidalgo. 42162. Distrito de Educación, Salud, Ciencia, Tecnología e Innovación, e-mail: jdgarcia@ipn.mx

A. González-Cisneros

Escuela Superior de Cómputo, Instituto Politécnico Nacional, Av. Juan de Dios Bátiz esq. Av. Miguel Othón de Mendizábal, Lindavista 07738, Gustavo A. Madero, Ciudad de México, México.

S. Molina-Valdovinos

Unidad Académica de Ciencia y Tecnología de la Luz y la Materia, Universidad Autónoma de Zacatecas, Circuito Marie Curie S/N, Parque de Ciencia y Tecnología QUANTUM Ciudad del Conocimiento, 98160, Zacatecas, Zacatecas, México.

D. Valdez-Perez

Instituto Politécnico Nacional, SEPI-ESIME, UPALM, Edif. Z-4 3er Piso, 07738, Ciudad de México, México.

A. A. Durán-Ledezma

SEPI, ESIME Ticomán, Instituto Politécnico Nacional, Av. Ticomán No. 600, San José Ticomán, 07340, Ciudad de México, México e-mail: aduranl@ipn.mx

Received 19 December 2024; accepted 12 June 2025

Ab initio DFT calculations were used to investigate how C, Ga, Ge, O, and Se doping modify the structural, electronic, and optical properties of arsenene. Our investigation has revealed that doping leads to substantial modifications in the electronic attributes and slight distortions in the crystal lattice, affecting bond lengths and angles. These modifications have led to tunable band gaps, which are vital for the development of nanoelectronic and optoelectronic technologies. Furthermore, we have delved into the optical properties of doped arsenene by calculating the dielectric function within the energy window of 0 to 10 eV. Our findings demonstrate that doping results in shifts in the absorption edges and changes in the refractive index. Overall, our results provide valuable insights into the tunability of electronic and optical characteristics in doped arsenene, paving the way for its implementation in advanced technological applications.

Keywords: Arsenene; doped arsenene; optical properties; density functional theory; dielectric function; refractive index; absorbance; density of states.

DOI: https://doi.org/10.31349/RevMexFis.71.061601

1. Introduction

Following the groundbreaking discovery of graphene, two-dimensional (2D) materials have transformed materials science, offering exceptional electronic, optical, and mechanical properties. Compared to bulk materials, 2D materials offer high adaptability for tunable applications due to their unique electronic structures and high surface-area-to-volume ratio [1]. 2D materials such as transition metal dichalcogenides (TMDs), phosphorene, and silicene have been produced for electronics, photonics, and optoelectronics applications [2,3].

Among these, in recent years, arsenene has garnered significant attention due to its potential applications in semiconductor photodetectors, LEDs, modulators, and advanced optoelectronic applications [3-6]. Arsenene is a single layer of arsenic atoms that can exist in different stable forms: buckled, puckered, and planar honeycomb structures [7-10]. Since 2016, there has been experimental evidence of monolayer-buckled arsenene [11] and multilayered arsenene nanoribbons [12]. A monolayer arsenene has an indirect band gap tunable to direct as the number of layers increases, under electric fields or by biaxial strain [7,8,13]. It has high carrier mobility [8], low anisotropic thermal conductivity [14], and chemical stability [10].

It is well known that adsorption and substitutional doping are feasible methods to change or improve two-dimensional materials, as well as mechanical, electronic, magnetic, and

optical properties [4,15-18]. Arsenene is not the exception; there have been reports of arsenene doped with different atoms, including C, O, B, N, S, Ga, Ge, P, Sb, Si, Sn, Se, Bi, Te, and F, among others [10]. The introduction of dopants into arsenene changes the electronic structure, creating new energy levels, and as a consequence, semiconductor, metallic, semimetallic, superconductor, and topological phases could be generated [10,19-25]. Moreover, doping caused a change in the bandgap of arsenene, going from indirect to direct [8,26-29]. On the other hand, doping can also enhance optical properties -such as dielectric function, absorption, and refractive index- to determine a material's light interactions and are essential in optimizing optoelectronic devices' performance [20,22,30-36]. Free-standing arsenene is a poorly efficient light emitter owing to the indirect bandgap, but under a minor strain and molecular doping, it experiences an indirect to direct bandgap transition [8,26-29,37]. Additionally, it was observed that in both single-layer and bilayer buckled arsenene, light absorption occurs within the visible-ultraviolet spectral range [29,32]. The adsorption of arsenene monolayer enhances optical absorption across the visible to near-infrared spectral range [36]. In arsenene nanoribbons along the zigzag and armchair edge, the imaginary parts of the dielectric function exhibit a redshift trend [31]. Arsenic-phosphorus compounds exhibit hexagonal (orthorhombic) phases, each possessing a wide bandgap with a value in the near-ultraviolet and visible regions of the electromagnetic spectrum, respectively [33]. Arsenene is functionalized with F, OH, and CH_3, and generates light absorption peaks in the near-infrared and visible regions of the solar spectrum [22]. Wang *et al.*, studied the modulated atomic substitution concentration of Al, Ga, and B into arsenene, generating a doping-dependent variation of the shear, bulk, and Young's modulus. Additionally, higher concentrations generate an anisotropic optical response, an increase in the static dielectric constant, and enlarged excited electron transitions between bands, which are reflected in the dielectric function, redshift in its absorption edge, and peak reflectance and valley transmittance values in the ultraviolet region [37].

Through Density Functional Theory (DFT) with Quantum Espresso, the effects of doping arsenene with carbon, oxygen, gallium, germanium, and selenium are investigated, chosen to explore both light and heavy dopants and their distinct impacts on optical properties and its dielectric response. We examine changes in the dielectric function across dopant types and concentrations. Absorbance, reflectivity, and transmittance, and their dopant dependence, are studied. Substitutional doping affects the band structure and, therefore, the optical absorption, absorbance, and dielectric response. This study aims to provide foundational insights for tailoring arsenene in next-generation optoelectronic devices.

This work is structured as follows: Section 2 provides a detailed description of the calculation methods, and the results are presented and discussed in Sec. 3. This section also includes the geometry stability, electronic structure, dielectric function, refractive index, absorbance, reflectivity, and transmittance. Finally, the conclusions are presented in Sec. 4.

2. Calculation methods

The Quantum Espresso software package [38-40] is used to perform first-principles calculations to investigate the structural and optical properties of arsenene and its doped variants, with exchange-correlation effects treated within the Generalized Gradient Approximation (GGA) [41]. We adopted Troullier-Martins pseudopotentials in conjunction with the Perdew-Burke-Ernzerhof (PBE) exchange-correlation functional. While the PBE functional provides a computationally efficient framework, it is known to underestimate band gap values. To obtain a more accurate representation of the electronic structure, closely aligned with experimental observations, we also employed the HSE06 hybrid functional, despite its increased computational demand [42,43]. The results derived from both functionals exhibit qualitative consistency, particularly in revealing doping-induced electronic states. Nevertheless, the calculated values of the intrinsic band gap and the pseudo-band gap vary depending on the functional employed, highlighting the influence of the chosen computational approach on the quantitative outcomes.

The system under consideration is an arsenene supercell of $4 \times 4 \times 1$ with a 20 Å vacuum layer in the z-direction to prevent periodic interactions between layers, Fig. 1a). A unit cell is used in all cases, with the lattice constants set to $a = b$. Moreover, one As atom in the Arsenene supercell is substituted by a single atom of D=C, Ga, Ge, O, and Se, corresponding to a substitution concentration of 3.13%. Figure 1b) shows a particular case of $3 \times 3 \times 1$ arsenene supercell substitutionally doped with D atoms (black sphere) corresponding to a concentration of 5.6% (illustrative case, not shown in the results). Arsenene has three structures (puckered, planar, and buckled); in all subsequent calculations, the buckled configuration is only considered. The plane-wave cut-off energy is set to 612 eV, and the electronic energy convergence criterion is defined as 1.36×10^{-9} eV. A $5 \times 5 \times 1$ Monkhorst-Pack k-point grid is employed for Brillouin zone sampling. Structural optimization is performed with a force convergence threshold of 1.36×10^{-5} eV/Bohr, and the residual stress is reduced to below 0.005 GPa. The total energy convergence criterion for the electronic self-consistent field (SCF) calculations is set to 1.36×10^{-5} eV. For calculations involving optical properties, a tighter threshold of 1.36×10^{-9} eV is used to ensure greater numerical accuracy.

3. Results and discussion

3.1. Geometry stability and electronic structure

The electronic structure and optical properties of the doped systems require an optimization of the atomic configurations

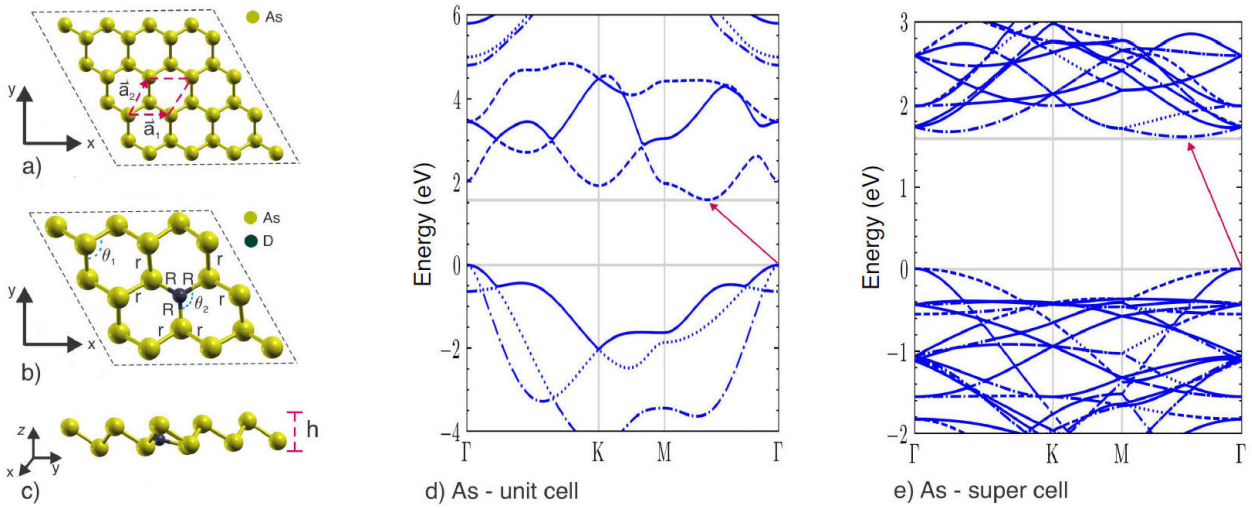

FIGURE 1. a) Top view of atomic model of freestanding $4 \times 4 \times 1$ super cell structure of arsenene. b) Illustration of $3 \times 3 \times 1$ arsenene super cell substitutionally doped with D = C, O, Ge, Se, or Ga (black sphere) to a concentration of 5.6%. In the case of a $4 \times 4 \times 1$ super cell, the doping concentration is reduced to 3.13%. c) Side view of a $3 \times 3 \times 1$ arsenene super cell substitutionally doped. Note that the doped atom has a height different from the arsenene atoms. d) and e) show the band structure computed with PBE of pristine monolayer arsenene for the unit cell and the $4 \times 4 \times 1$ super cell, respectively. The red line indicates the indirect band gap ~ 1.61 eV.

and dimensions of the lattice supercell. In comparison to arsenene, the crystalline architecture of doped systems exhibits alterations; therefore, the symmetry of arsenene is no longer present. Table I lists the geometric parameters: lattice constants a, As-D bond lengths and angle (R, θ_2), As-As bond lengths and angle (r, θ_1). The first row corresponds to pristine arsenene as a reference. After doping and the optimization process, the values of the lattice constants are presented in the first column; it is possible to appreciate a slight variation of the lattice parameter compared to the pristine arsenene. When doping with O and C atoms, a reduction in the lattice parameter is present, indicating a compaction of the structure; however, for doping with Ga, Ge, and Se atoms, there is an increase in the parameter, indicating an expansion. The bond lengths R (As-D) for the O, C, Ga, and Ge dopants are shorter than the As-As bonds for the pristine arsenene (2.52 Å), thus generating stronger bonds with arsenic, contrary to that obtained for Se, which presents an $R = 2.57$ Å being higher than pristine arsenene, indicating a weaker bond. θ_1 (As-D bond angle) is larger for all dopants, generating a loss of symmetry; θ_1 (As-As bond angle) presents very slight changes for most of the dopants, except for O, where the variation at $88.7°$ is very noticeable, highly related to the corresponding bond length results from R. Finally, the last two columns are related to the bandgap (E_g) computed with the PBE and HSE06. The PBE approximation generates a decrease in the bandgap for all dopants, suggesting the generation of new electronic states near the valence band or the conduction band, thus reducing the bandgap. For As, C, Ge, O, Se, and Ga, the pseudo bandgap values are 1.61 eV, 0.61 eV, 0.42 eV, 0.52 eV, 1.13 eV, and 1.47 eV, respectively. The reported values correspond to the energy difference between the bottom of the impurity band and the valence band maximum. As we can see, the PBE functional underestimates the band gap values of the doping cases. The last column displays the more accurate band gap values obtained with the implementation of the HSE06 hybrid functional potentials. In the same column, the band gap values are compared with those of Ref. [28].

TABLE I. Structural parameters of arsenene supercell and the doped systems. The different columns show the lattice constants a, As-D bond lengths (R), As-As bond length (r), As-D and As-As bond angles (θ_1 and θ_2). The first row corresponds to the arsenene monolayer as a reference, and the last two columns show the band gap performed with PBE and HSE06.

Dopant atom	a (Å)	R (Å)	r (Å)	θ_1 (°)	θ_2 (°)	E_g (eV) / PBE	E_g (eV) / HSE
As	14.40	2.52	2.52	91.9	91.9	1.61	2.03/2.21[a]
C	14.37	1.98	2.56	89.7	114.19	0.61	0.83/1.36[a]
Ge	14.57	2.49	2.51	93.1	103.6	0.42	0.59/1.24[a]
O	14.23	2.09	2.50	88.7	110.7	0.52	0.93/- -[a]
Se	14.54	2.57	2.50	92.2	105.3	1.13	1.50 /- -[a]
Ga	14.56	2.45	2.51	93.7	117.2	1.47	1.90/2.06[a]

[a] Reference [28]

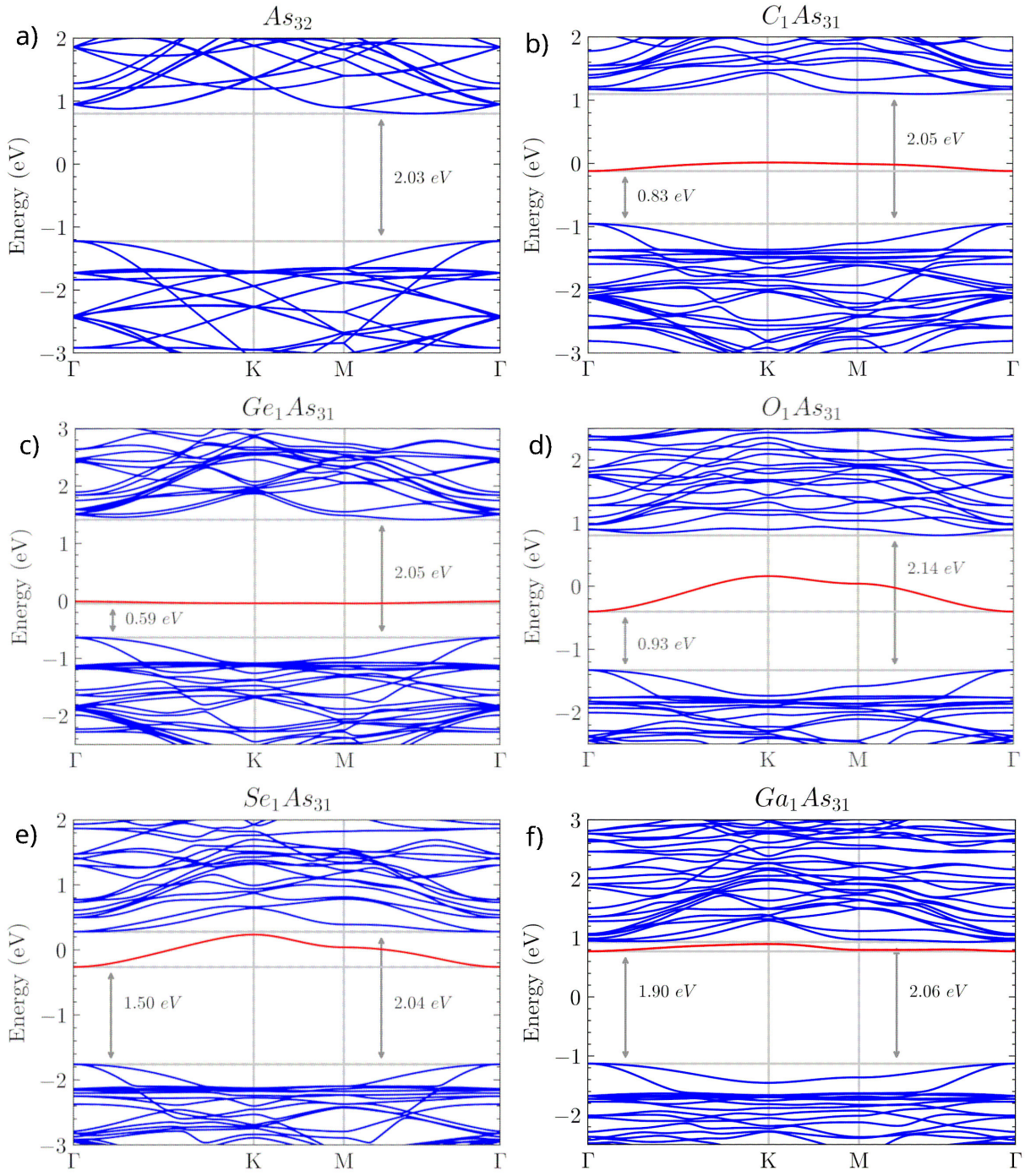

FIGURE 2. The band structures of doped arsenene are calculated using HSE06 hybrid functional potentials. The different figures correspond to a) pristine arsenene and arsenene doped with b) C, c) Ge, d) O e) Se, and f) Ga. The red line indicates the band associated with the doped element.

The band structure computed with PBE of arsenene unit cell and $4 \times 4 \times 1$ supercell is shown in Figs. 1d) and 1e), respectively. The arsenene exhibits semiconducting behavior with an indirect band gap of 1.61 eV. The top of the valence band is located at the Γ point, and the bottom of the conduction band is between the M and Γ points. Figures 2a)-2f) display the band structure obtained from the HSE06 hybrid functional potentials of pristine arsenene and C, Ge, O, Se, and Ga-doped systems. The more accurate band gap for As obtained from HSE06 is around 2.03 eV. As we can see, PBE and HSE06 generate similar band structures for As except for the band gap. Ga dopants transform arsenic from an indirect band to a direct band at the Γ point, which improves its ability to absorb and emit light. The Ga dopant atoms are closer than the conduction band, resulting in an n-type semiconductor. The Ga band gap is around 1.90 eV with HSE06, see

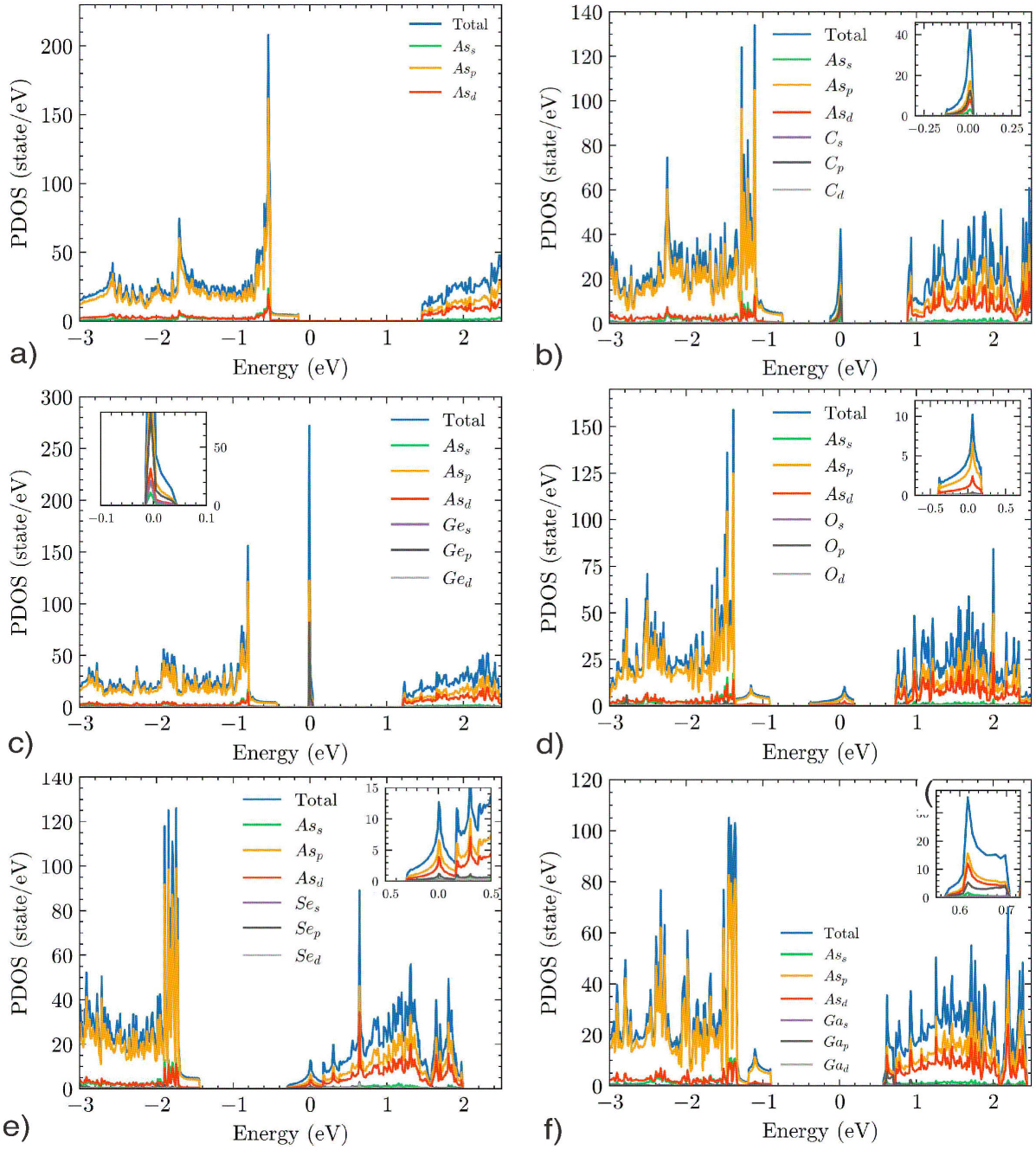

FIGURE 3. Total density of states (TDOS, blue line) and partial density of states (PDOS) of arsenene a) and arsenene substitutionally doped with b) C, c) Ge, d) O, e) Se, and f) Ga.

Fig. 2f). C and Ge show an indirect band gap around 0.83 eV and 0.59 eV, respectively, see Figs. 2b) and 2c). For their part, O and Se have a semimetallic contribution from dopant atoms crossing the Fermi energy, see Figs. 2d) and 2e). Additionally, dopants such as O and C generate more significant distortions in the band structure due to their high electronegativity. As seen in the figures, there are visible variations in the curvatures of the bands; for Ga, the curvatures are a little more pronounced, indicating lighter carriers and greater mobility, contrary to Ge, which has flatter bands, implying heavier carriers and lower mobility.

Figure 3 shows the total density of states (TDOS, blue line) and partial density of states (PDOS) for As_{32}, C_1As_{31}, Ga_1As_{31}, Ge_1As_{31}, O_1As_{31}, and Se_1As_{31} doping systems. In Fig. 3a) (As) The hybridization of As_{4p} orbitals is evident, with dominant contributions in the range of -1.4 eV to -1 eV. A bandgap of 1.61 eV is observed, consistent with the values reported in the literature [28]. In the conduction band, As_{4p} orbitals exhibit higher density than As_{3d}, whereas both orbitals contribute nearly equally in the valence band. The valence band lies closer to the Fermi energy, indicating p-type semiconductor behavior. As observed in Fig. 3b) the

DOS of C_1As_{31} can be divided into two regions, the first one from -0.2 eV to 0 eV, the states are primarily composed of As_{4p}, with minor contributions from C_{2s} and C_{2p}, attributed to trigonal pyramidal bonding and the influence of dangling bonds or lone-pair electrons, which reduce the bandgap. The second region is from -3 eV to -0.6 eV; in this region, the As_{4p} orbitals dominate due to system hybridization. Figure 3c) shows the case of Ge_1As_{31}, here the As_{4p} remains dominant due to the trigonal pyramidal bonding and induces states near the Fermi level. The reduced gap between valence and conduction bands suggests p-type behavior, contrasting with prior dopants. In Fig. 3d), the O_1As_{31} exhibits a valence band with As_{4p} hybridization and weaker trigonal pyramidal effects compared to C or Ge doping. The conduction band shifts closer to the Fermi level compared to pure As, resulting in n-type semiconductor behavior, with states mainly derived from As_{4p} and As_{3d}, and negligible oxygen contribution. The conduction band behavior aligns with C_1As_{31} and Ge_1As_{31}. In the case of Se_1As_{31} in Fig. 3e), the DOS shifts away from the valence band, retaining As_{4p} hybridization. Trigonal pyramidal effects are visible. Simultaneously, electron occupation near the conduction band minimum leads to carrier degeneracy, forming a semimetallic behavior with enhanced electrical properties. Finally, Ga_1As_{31}, Fig. 3f), the valence band in the range -1.6 to -1.2 eV is dominated by As_{4p} orbitals, showing hybridization similar to previous systems. The conduction band resembles C_1As_{31}, but with a stronger shift toward the Fermi energy, confirming n-type characteristics.

3.2. The dielectric function

The optical response of a material is given by its complex dielectric function ε, which is defined by the expression

$$\varepsilon = \varepsilon_1 + i\varepsilon_2. \tag{1}$$

The real part of the dielectric function ε_1 represents the degree of polarization of the material under an external electric field. So, a larger real part implies a stronger polarization capability of the material. On the other hand, the imaginary dielectric function ε_2 represents the absorption capacity of the material at a specific energy. When light passes through a solid material, the photons interact with electrons, ions, or atoms. In the case of semiconductors, if the photon energy is equal to or greater than the bandgap, then electrons in the valence band absorb light, promoting the generation of pairs of electron holes. In the generation processes, the electrons are promoted from the valence band to the conduction band.

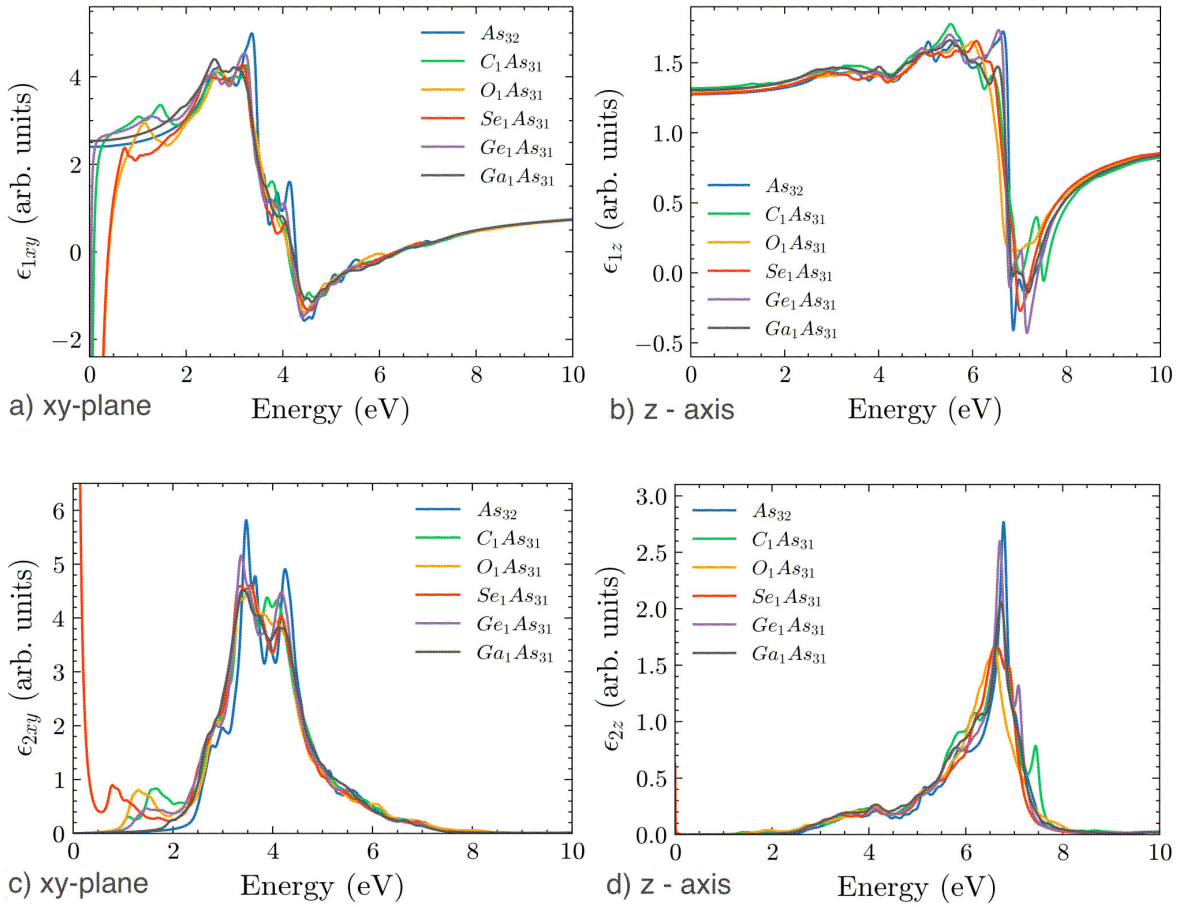

FIGURE 4. a)-b) Real and c)-d) imaginary parts of the dielectric function $\varepsilon(\omega)$ of arsenene substituted with Ga, Ge, O, Se, and C atoms along the xy-plane and z-axis, respectively.

The real and imaginary parts of the dielectric function written in terms of angular frequency ω are related by the Kramers-Kröning equations

$$\varepsilon_1(\omega_0) = 1 + \frac{2}{\pi}\mathbf{P}\int_0^\infty d\omega \frac{\omega\varepsilon_2(\omega)}{\omega^2-\omega_0^2}, \tag{2}$$

$$\varepsilon_2(\omega_0) = \frac{2\omega_0}{\pi}\mathbf{P}\int_0^\infty d\omega \frac{\varepsilon_1(\omega-1)}{\omega_0^2-\omega^2}, \tag{3}$$

where $\mathbf{P}$ indicates a Cauchy principal integral [44]. On the other hand, the imaginary dielectric function can be calculated using the expression given in Ref. [45].

To investigate the optical properties of the substituted systems, the dielectric function for each material is calculated, as shown in Fig. 4. The real part of the dielectric function, Figs. 4a) and 4b), shows that the atom substitutions modify slightly the polarization capability of the arsenene system. The photon energy turns negative when it surpasses 3.86 eV along the xy-plane and 6.48 eV along the z-axis, signifying a reduced capacity of the system to bind electrons. Figure 4c) shows the imaginary part of the dielectric function along the xy-plane. We can see that all systems have the maximum peak around the same photon energy. Also, the substituted atoms weaken the photon absorption ability of arsenene in the range $2.8 - 4.2$ eV, and all systems can absorb photons when the photon energy is between 0 and 2 eV. Additionally, the system's dielectric function is anisotropic up to a photon energy of 10 eV and isotropic above this barrier. In the same way, the imaginary part along the z-axis shows a maximum value around 7 eV for As_{32}. The incorporation of dopant elements reduces the maximum value according to the band gap value; *i.e.*, the elements with the largest band gap exhibit the maximum value, and as the band gap is reduced, the maximum peak also decreases.

3.3. Real refractive index

The real refractive index can be computed by the expression [46]

$$n = \sqrt{\frac{1}{2}\left(\varepsilon_1 + \sqrt{\varepsilon_1^2+\varepsilon_2^2}\right)}. \tag{4}$$

This refractive index measures how electromagnetic radiation curves when it passes from one material to another, and it is influenced by the material's ability to absorb electromagnetic radiation [47].

The refractive index and its dependence on the energy are shown in Fig. 5. When the dopants are incorporated, the refractive index values in the xy-plane increase in the region of near UV or high wavelengths. The C, O, and Ge dopants show the highest values, consistent with the previous behavior observed for ε_{1xy}. Posteriorly, the refraction index achieves its maximum value in the visible region for all the dopant systems, revealing its high interaction with visible light. Finally, for wavelengths in the UV region, the figure clearly shows the minimum value for the refractive index, a behavior related to the absorption coefficient ε_2. On the contrary, the refractive index along the z-axis shows its maximum in the far ultraviolet region according to ε_{1z}.

The static refractive index $n|_{E=0}$ following the relation

$$n|_{E=0} = \sqrt{\varepsilon_1|_{E=0}}, \tag{5}$$

where $\varepsilon_1|_{E=0}$ is the static dielectric constant. Table II shows the main values for the static refractive index and the static dielectric constant for arsenene and doped systems in the xy-plane and the z-axis, respectively.

3.4. Energy-loss function

The energy-loss function (ELF) reflects the probability of how an electron loses energy and transfers momentum when traveling a unit path into a solid [48]. The ELF relates to

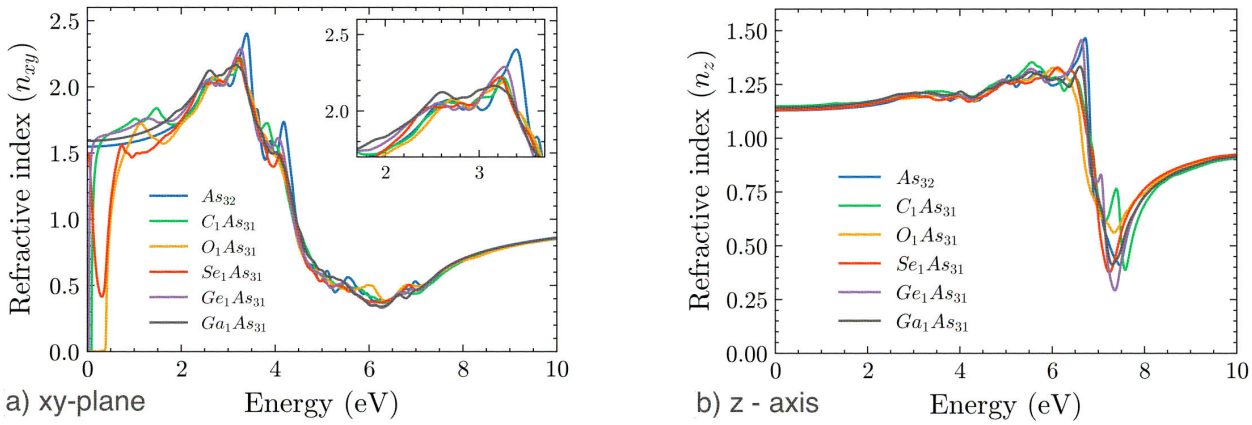

FIGURE 5. Refraction index as a function of the energy for arsenene and doped systems along the a) xy-plane and b) z-axis.

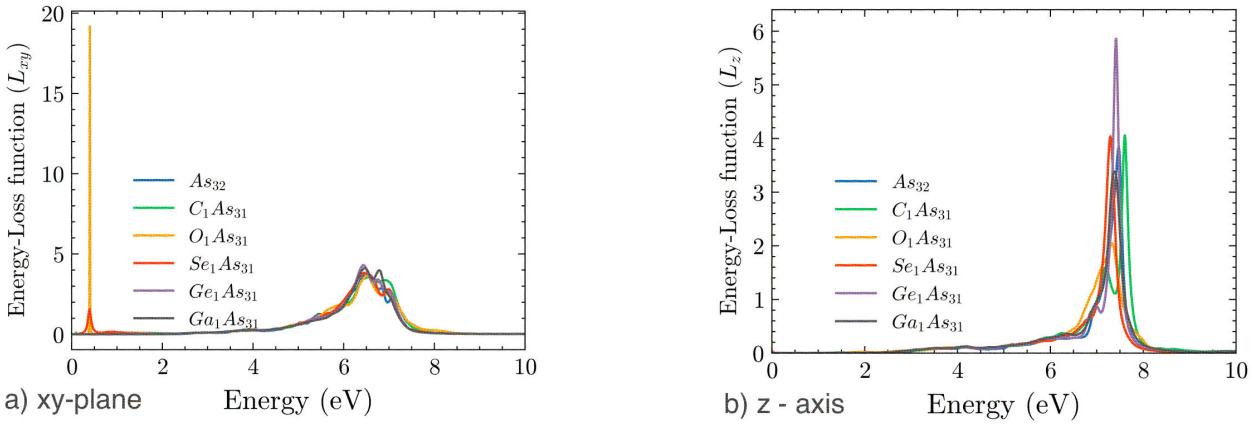

FIGURE 6. Energy-loss spectrum for arsenene and doped systems along the a) xy-plane and b) z-axis.

the imaginary component of the reciprocal complex dielectric function, and it is defined as:

$$L = \text{Im}\left(\frac{-1}{\varepsilon}\right) = \frac{\varepsilon_2}{\varepsilon_1^2 + \varepsilon_2^2}. \tag{6}$$

By implementing Eq. (6), we calculate the energy-loss function for zero exchanged momentum, as shown in Fig. 6. The doping effect is illustrated in two configurations: in the xy-plane and along the z-axis. In the xy-plane Fig. 6a), all the principal absorption peaks remain located in the ultraviolet region (around 180 nm). No significant shifts in peak positions are observed relative to pure arsenene, and the overall spectral profile remains largely unchanged. These main peaks in the ELF result from the second zeros of real dielectric functions and can be explained within the free-electron-plasmon picture. The main difference is in intensity, principally in the O-doped system; the electronegativity introduces a redistribution of the electric charge, which reduces the density of free electrons, reducing the plasmonic response. In Fig. 6b), the behavior in the z-direction is presented; here, although the peaks are in the UV region, there are soft changes in the positions, shapes, and intensities. The C-doped system presents a considerable shift; the position shift is related to introducing new energetic levels, modifying the collective frequency with which the plasmon interacts, and shifting to different energies. All of this is consistent with the optical anisotropy of the system present in the z-direction.

TABLE II. Static dielectric constant ($\varepsilon_1|_{E=0}$) and static refractive index ($n|_{E=0}$) for arsenene and doped systems in the xy-plane and z-axis.

Doped atom	$\varepsilon_{1xy}\|_{E=0}$	$\epsilon_{1z}\|_{E=0}$	$n_{xy}\|_{E=0}$	$n_z\|_{E=0}$
As	2.40	1.28	1.55	1.13
C	- -	1.45	0	1.20
Ga	2.53	1.31	1.59	1.14
Ge	-3754.41	1.29	0	1.14
O	- -	2.35	0	1.53
Se	- -	0	0	0.79

3.5. Absorbance, reflectivity and transmittance

When electromagnetic radiation hits a material, this radiation can be absorbed, reflected, or transmitted. In general, reflection, transmission, and absorption depend on the wavelength of the incident radiation [49,50]. The reflectivity of an arbitrary system is defined as

$$R = \left|\frac{\sqrt{\varepsilon} - 1}{\sqrt{\varepsilon} + 1}\right|^2. \tag{7}$$

Figure 7 shows the reflectivity of arsenene and doped systems versus energy along the xy-plane and z-axis. It can be seen that the reflectivity R_{xy} reaches its perfect maximum values near $E = 0$ eV, these values correspond to the response of the doped elements C, O, Se, and Ge. A constant reflectivity $R_{xy} \approx 5$ is observed for both Ga and As in the $0 - 1$ eV range, which is associated with the absence of doping-induced states in this region. From energies above 1 eV, the reflectivity begins to rise in all cases, reaching its highest values between 3 and 6 eV. The reflectivity exhibited by doped systems surpasses that of arsenene when subjected to infrared radiation (IR). For energies $E > 7$ eV, the reflectivity decreases going to zero, corresponding to a longer wavelength than 900 nm. The reflectivity along the z-axis takes its maximum values in the energy range of 6 eV $< E <$ 8 eV, surprisingly the Ge doped element shows the maximum response 38%, followed by Se (28%), Ga (26.2%), As (26%), C (25%), and O (14%).

The following equation obtains the layer-dependent absorbance

$$A = \frac{2\pi}{\lambda} L\varepsilon_2, \tag{8}$$

where λ is the wavelength of the incident radiation and L is the total size of the cell along lattice vector $\vec{c}$.

The absorbance for the systems is represented in Fig. 8. The xy absorbance for the pure arsenene and doped systems is shown in Figs. 8a). The absorbance peaks corresponding to pure arsenene exhibit greater sharpness and intensity

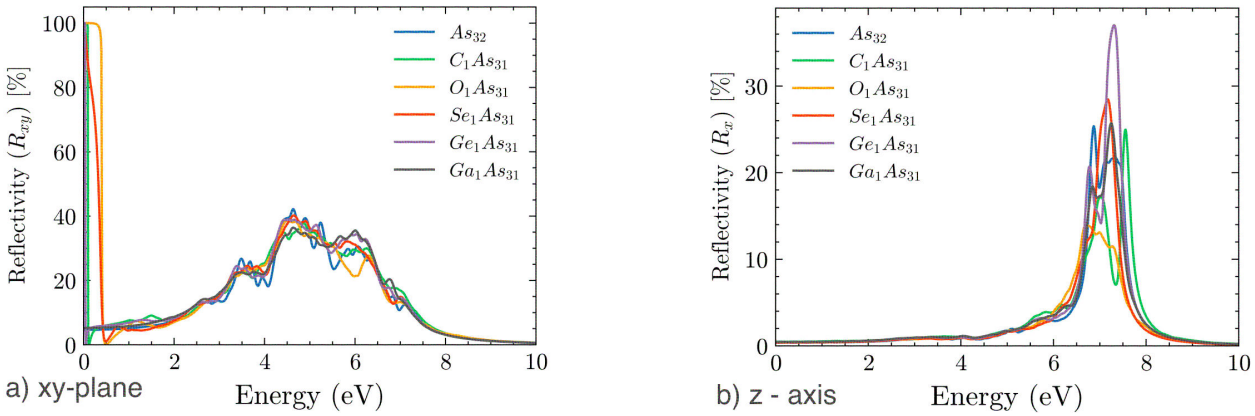

FIGURE 7. Reflectivity as a function of energy for arsenene and doped systems along the a) xy-plane and b) z-axis.

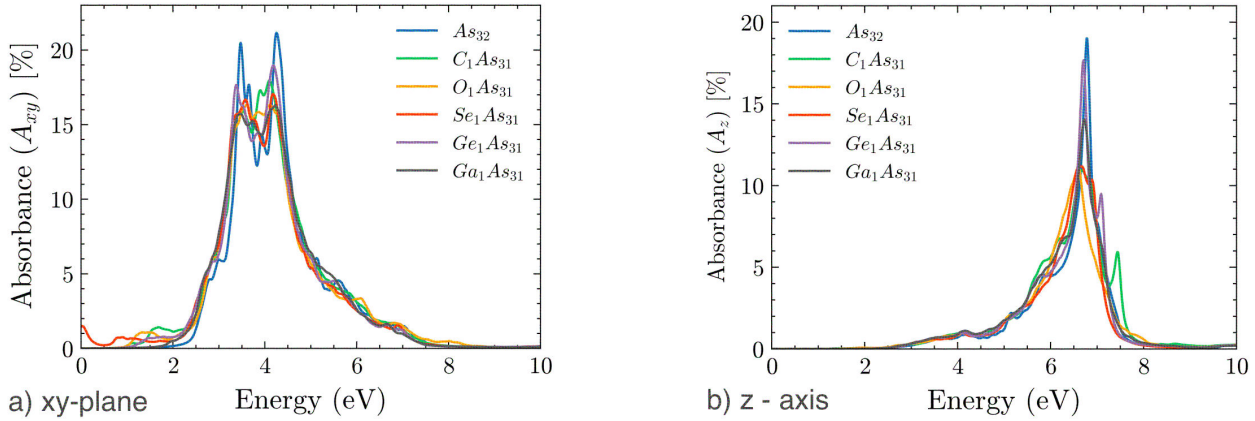

FIGURE 8. Absorbance as a function of the energy along the a) xy-plane and b) z-axis.

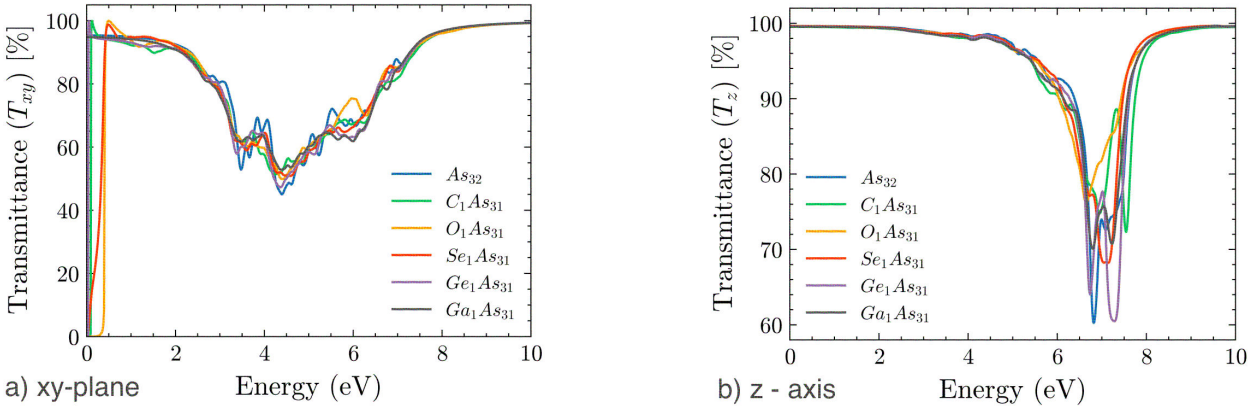

FIGURE 9. Transmittance as a function of the energy along the a) xy-plane and b) z-axis.

compared to those of the doped systems; the incorporation of dopants results in a consistent shape, albeit accompanied by a decrease in intensity attributable to alterations in the electronic structure. Furthermore, the peak absorbance values for the examined systems are situated within the ultraviolet spectrum, with the maximum recorded value being below 22%. For energies below 2 eV, there is an observed decrease in absorbance corresponding to an increase in wavelength; within the energy range of 3 eV to 5 eV, absorbance attains a maximum point. For energies exceeding 5 eV, absorbance diminishes until it effectively reaches zero. The absorbance of As, Ge, and Ga along the z-axis shows maximum values at a difference of the semimetallic elements Se, C, and O that present low absorbance. Finally, using the following relation

$$1 = A + R + T, \tag{9}$$

we compare the transmittance T for the systems, which are represented in Fig. 9. As expected, the transmittance in the xy-plane reaches its minimum value in the ultraviolet region or near to $E = 0$ eV. For energies $2\ \mathrm{eV} < E < 8\ \mathrm{eV}$ the transmittance shows low values, the value for the doped systems is higher than arsenene, which is more evident for C and Ge doped systems, caused by modification of the electronic density of the states and bandgap. After $E > 8\ \mathrm{eV}$ the transmittance grows until reaches the perfect value. For the z axis, Fig. 9b), the transmittance exhibits almost perfect value behavior for all systems from 0 eV to 4 eV, achieving a minimum near 7 eV. When the energy is in the range 5 eV to 8 eV, the transmittance reaches the minimum value in the following order: As, Ge, Se, Ga, C, and O. Whenever the energy $E > 8\ \mathrm{eV}$, the transmittance increases until its maximum value.

4. Conclusions

This work analyzed the effect of doping with C, Ge, Ga, O, and Se atoms over arsenene's structural, electrical, and optical properties through ab initio calculations, revealing insights into their potential applications in optoelectronic devices. Incorporating dopants alters the electronic band structure. Doping with O and C atoms generates a contraction, while doping with Ga, Ge, and Se atoms results in an expansion of the lattice. The band-gap changes from indirect to direct for Ga ($E_g = 2.06\ \mathrm{eV}$). The O and Se show a semimetallic behavior due to the creation of new electronic states or bands that cross the Fermi energy. While C ($E_g = 1.21\ \mathrm{eV}$) and Ge ($E_g = 1.46\ \mathrm{eV}$) preserves the indirect band gap. It was possible to observe how the dopants softly modify the polarization capacity in the xy-plane and along the z-axis, reducing the capacity of the system to bind electrons. The energy-loss function showed that plasmonic peaks remain in the UV region for the xy-plane. Still, in the z-direction, the intensity of the peaks presented variation for all systems and slight displacement, being C-doped, which presents the most considerable shift caused by increased free carrier density and the anisotropy of the material. Finally, the transmittance presents minimums in the UV region and maximums in the infrared region for C and Ge-doped systems. The findings suggest these dopants can optimize the optical performance of arsenene, making it a promising candidate for future technologies. Overall, ab initio methods provide a powerful framework for understanding and predicting the optical behavior of doped arsenene, paving the way for innovative applications in materials science.

Acknowledgements

This work was partially supported by EDD-IPN, EDI-IPN, Sistema Nacional de Investigadores (SNI-SECIHTI), and Instituto Politécnico Nacional (SIP-IPN Project Numbers 20240630, 20241177, and 20240691). A. A. Durán-Ledezma thanks SECIHTI for her postdoctoral fellowship.

1. J. Arun, N. Nirmala, and S. S. Dawn, Environmental Applications of Carbon-Based Materials (IGI Global, 2024).
2. K. M. Neilson et al., Toward Mass Production of Transition Metal Dichogenide Solar Cells: Scalable Growth of Photovoltaic-Grade Multilayer WSe2 by Tungsten Selenization, *ACS Nano* **18** (2024) 24819, https://doi.org/10.1021/acsnano.4c03590.
3. D. S. Aditya and S. K. Nataraj, Structural, optical, and electronic properties of twodimensional nanomaterials, in Two-Dimensional Nanomaterials-Based Polymer Nanocomposites (John Wiley and Sons, Ltd, 2024) Chap. 5, pp. 167-194.
4. P.-C. Chen *et al*., High-Performance Single-Crystalline Arsenic-Doped Indium Oxide Nanowires for Transparent Thin-Film Transistors and Active Matrix Organic Light-Emitting Diode Displays, *ACS Nano* **3** (2009) 3383, https://doi.org/10.1021/nn900704c.
5. S. S. Dongre *et al*., Review on 2D Arsenene and Antimonene: Emerging Materials for Energy, Electronic and Biological Applications, *Adv. Mater. Interfaces* **9** (2022) 2200442, https://doi.org/10.1002/admi.202200442.
6. X.-J. Ye, G.-L. Zhu, J. Liu, C.-S. Liu, and X.-H. Yan, Monolayer, Bilayer, and Heterostructure Arsenene as Potential Anode Materials for Magnesium-Ion Batteries: A First-Principles Study, *J. Phys. Chem. C* **123** (2019) 15777, https://doi.org/10.1021/acs.jpcc.9b02399.
7. C. Kamal and M. Ezawa, Arsenene: Two-dimensional buckled and puckered honeycomb arsenic systems, *Phys. Rev. B* **91** (2015) 085423, https://doi.org/10.1103/PhysRevB.91.085423.
8. S. Zhang, Z. Yan, Y. Li, Z. Chen, and H. Zeng, Atomically Thin Arsenene and Antimonene: Semimetal-Semiconductor and Indirect-Direct Band-Gap Transitions, *Angew. Chem. Int. Ed.* **54** (2015) 3112, https://doi.org/10.1002/anie.201411246.
9. S. Zhang *et al*., Semiconducting Group 15 Monolayers: A Broad Range of Band Gaps and High Carrier Mobilities, *Angew. Chem. Int. Ed.* **55** (2015) 1666, https://doi.org/10.1002/anie.201507568.
10. J. Zhao, Z.-H. Qi, Y. Xu, J. Dai, X. C. Zeng, W. Guo, and J. Ma, Theoretical studies on tunable electronic structures and potential applications of two-dimensional arsenene-based materials, *WIREs Comput. Mol. Sci*. **9** (2018) e1387, https://doi.org/10.1002/wcms.1387.

11. J. Shah, W. Wang, H. M. Sohail, and R. I. G. Uhrberg, Experimental evidence of monolayer arsenene: an exotic 2D semiconducting material, *2D Mater.* **7** (2020) 025013, https://doi.org/10.1088/2053-1583/ab64fb.

12. H.-S. Tsai, S.-W. Wang, C.-H. Hsiao, C.-W. Chen, H. Ouyang, Y.-L. Chueh, H.-C. Kuo, and J.-H. Liang, Direct Synthesis and Practical Bandgap Estimation of Multilayer Arsenene Nanoribbons, *Chem. Mater.* **28** (2016) 425, https://doi.org/10.1021/acs.chemmater.5b04949.

13. S. Zhang, Z. Yan, Y. Li, Z. Chen, and H. Zeng, Atomically Thin Arsenene and Antimonene: Semimetal-Semiconductor and Indirect-Direct Band- Gap Transitions, Angew. *Chem. Int. Ed.* **54** (2015) 3112, https://doi.org/10.1002/anie.201411246.

14. M. Zeraati, S. M. Vaez Allaei, I. Abdolhosseini Sarsari, M. Pourfath, and D. Donadio, Highly anisotropic thermal conductivity of arsenene: An ab initio study, *Phys. Rev. B* **93** (2016) 085424, https://doi.org/10.1103/PhysRevB.93.085424.

15. P. Rastogi, S. Kumar, S. Bhowmick, A. Agarwal, and Y. S. Chauhan, Effective Doping of Monolayer Phosphorene by Surface Adsorption of Atoms for Electronic and Spintronic Applications, *IETE J. Res.* **63** (2017) 205, https://doi.org/10.1080/03772063.2016.1243020.

16. V. V. On, C. V. Ha, D. T. Anh, J. Guerrero-Sanchez, and D. M. Hoat, Designing doping strategy in arsenene monolayer for spintronic and optoelectronic applications: a case study of germanium and nitrogen as dopants, *J. Phys.: Condens. Matter* **34** (2022) 355301, https://doi.org/10.1088/1361-648X/ac7a81.

17. Y. Li, C. Xia, T. Wang, X. Tan, X. Zhao, and S. Wei, Light adatoms influences on electronic structures of the two-dimensional arsenene nanosheets, *Solid State Commun.* **230** (2016) 6, https://doi.org/10.1016/j.ssc.2016.01.005.

18. A. A. Kistanov, S. Kh. Khadiullin, S. V. Dmitriev, and E. A. Korznikova, A First-Principles Study on the Adsorption of Small Molecules on Arsenene: Comparison of Oxidation Kinetics in Arsenene, Antimonene, Phosphorene, and InSe, *Chem. Phys. Chem* **20** (2018) 575, https://doi.org/10.1002/cphc.201801070.

19. M.-Y. Liu, Y. Huang, Q.-Y. Chen, C. Cao, and Y. He, Unexpected electronic structure of the alloyed and doped arsenene sheets: First-Principles calculations, *Sci. Rep.* **6** (2016) 29114, https://doi.org/10.1038/srep29114.

20. X. Liu, L. Liu, L. Yang, X. Wu, and P. K. Chu, Optical Identification of Topological Defect Types in Monolayer Arsenene by First-Principles Calculation, *J. Phys. Chem. C* **120** (2016) 24917, https://doi.org/10.1021/acs.jpcc.6b10303.

21. X. Kong, M. Gao, X.-W. Yan, Z.-Y. Lu, and T. Xiang, Superconductivity in electron-doped arsenene, *Chin. Phys. B* **27** (2018) 046301, https://doi.org/10.1088/1674-1056/27/4/046301.

22. J. Zhao, Y. Li, and J. Ma, Quantum spin Hall insulators in functionalized arsenene (AsX, X = F, OH and CH3) monolayers with pronounced light absorption, *Nanoscale* **8** (2016) 9657, https://doi.org/10.1039/C6NR01683A.

23. M. Qi, S. Dai, and P. Wu, Tuning electronic structure and magnetic properties of Mn- and Fe-doped arsenene with biaxial strain, *J. Phys.: Condens. Matter* **32** (2019) 085802, https://doi.org/10.1088/1361-648X/ab537a.

19

24. D.M. Hoat *et al.*, Developing feature-rich electronic and magnetic properties in the ß-As monolayer for spintronic and optoelectronic applications by C and Si doping: A first-principles study, *Surf. Interfaces* **27** (2021) 101534, https://doi.org/10.1016/j.surfin.2021.101534.

25. J. Du, C. Xia, T.Wang, X. Zhao, X. Tan, and S.Wei, First-principles studies on substitutional doping by group IV and VI atoms in the two-dimensional arsenene, *Appl. Surf. Sci* . **378** (2016) 350, https://doi.org/10.1016/j.apsusc.2016.03.055.

26. J. He, G. Liu, X. Li, H. Wang, and G. Zhang, First-principles study of strain on BN-doped arsenene, *J. Mol. Modeling* **28** (2022) 190, https://doi.org/10.1007/s00894-022-05186-9.

27. M. Bai, W.X. Zhang, and C. He, Mechanical, Electronic and magnetic properties of Ga, Ge, P and Sb doped monolayer arsenene, *J. Solid State Chem.* **251** (2017) 1, https://doi.org/10.1016/j.jssc.2017.04.004.

28. Z. Liu *et al.*, First-principles study of structural and electronic properties of substitutionally doped arsenene, *Physica E* **119** (2020) 114018, https://doi.org/10.1016/j.physe.2020.114018.

29. D. Kecik, E. Durgun, and S. Ciraci, Stability of single-layer and multilayer arsenene and their mechanical and electronic properties, *Phys. Rev. B* **94** (2016) 205409, https://doi.org/10.1103/PhysRevB.94.205409.

30. J. M. Galicia Hernandez, H. N. Fernandez-Escamilla, J. Guerrero Sanchez, and N. Takeuchi, Electronic and optical properties of the buckled and puckered phases of phosphorene and arsenene, *Sci. Rep.* **12** (2022) 20979, https://doi.org/10.1038/s41598-022-24425-w.

31. Y.-L. Song, D.-B. Lu, and X.-Y. Huang, Optical properties of arsenene nanoribbons: A first principle study, *Mater. Sci. Semicond. Process.* **136** (2021) 106139, https://doi.org/10.1016/j.mssp.2021.106139.

32. D. Kecik, E. Durgun, and S. Ciraci, Optical properties of single-layer and bilayer arsenene phases, *Phys. Rev. B* **94** (2016) 205410, https://doi.org/10.1103/PhysRevB.94.205410.

33. J. M. Galicia Hernandez, J. Guerrero-Sanchez, J. A. Rodriguez-Martinez, and N. Takeuchi, First-Principles Studies of the Electronic and Optical Properties of Two-Dimensional Arsenic-Phosphorus (2D As-P) Compounds, *ACS Omega* **9** (2024) 35718, https://doi.org/10.1021/acsomega.4c04108.

34. H. Shu, Y. Li, X. Niu, and J. Guo, Electronic structures and optical properties of arsenene and antimonene under strain and an electric field, *J. Mater. Chem. C* **6** (2018) 83, https://doi.org/10.1039/C7TC04072E.

35. D. Singh, S. K. Gupta, Y. Sonvane, and S. Sahoo, Modulating the electronic and optical properties of monolayer arsenene phases by organic molecular doping, *Nanotechnology* **28** (2017) 495202, https://doi.org/10.1088/1361-6528/aa9430.

36. M. Sun, J.-P. Chou, J. Gao, Y. Cheng, A. Hu, W. Tang, and G. Zhang, Exceptional Optical Absorption of Buckled Arsenene Covering a Broad Spectral Range by Molecular Doping, *ACS Omega* **3** (2018) 8514, https://doi.org/10.1021/acsomega.8b01192.

37. J. X. Wang, G. L. Liu, L. Wei, and G. Y. Zhang, First-principles calculations to investigate the effect of X (X=B, Al, Ga) atomic substitution concentration on the electronic structure and optical properties of arsenene, *Mod. Phys. Lett. B* **38** (2024) 2450095, https://doi.org/10.1142/S0217984924500957.

38. P. Giannozzi *et al*., Advanced capabilities for materials modelling with Quantum ESPRESSO, *J. Phys.: Condens. Matter* **29** (2017) 465901, https://doi.org/10.1088/1361-648X/aa8f79.

39. P. Giannozzi *et al*., QUANTUM ESPRESSO: a modular and open-source software project for quantum simulations of materials, *J. Phys.: Condens. Mat- ter* **21** (2009) 395502, https://doi.org/10.1088/0953-8984/21/39/395502.

40. P. Giannozzi *et al.*, Quantum ESPRESSO toward the exascale, *The Journal of Chemical Physics* **152** (2020) 154105, https://doi.org/10.1063/5.0005082.

41. N. T. Hung, A. R. T. Nugraha, and R. Saito, Quantum ESPRESSO Course for Solid-State Physics (Jenny Stanford Publishing Pte. Ltd., Singapore, 2023), https://doi.org/10.1201/9781003290964.

42. J. Heyd, G. E. Scuseria, and M. Ernzerhof, Hybrid functionals based on a screened Coulomb potential, *J. Chem. Phys.* **118** (2003) 8207, https://doi.org/10.1063/1.1564060.

43. A. V. Krukau, O. A. Vydrov, A. F. Izmaylov, and G. E. Scuseria, Influence of the exchange screening parameter on the performance of screened hybrid functionals, *J. Chem. Phys.* **125** (2006) 224106, https://doi.org/10.1063/1.2404663.

44. J. Piprek, Semiconductor Optoelectronic Devices: Introduction to Physics and Simulation (Academic Press, 2003).

45. C. Ambrosch-Draxl and J. O. Sofo, Linear optical properties of solids within the full-potential linearized augmented planewave method, *Comput. Phys. Commun*. **175** (2006) 1, https://doi.org/10.1016/j.cpc.2006.03.005.

46. S. Saha, T. P. Sinha, and A. Mookerjee, Electronic structure, chemical bonding, and optical properties of paraelectric $BaTiO_3$, *Phys. Rev. B* **62** (2000) 8828, https://doi.org/10.1103/PhysRevB.62.8828.

47. H. M. Gomaa, I.S. Yahia, and H.Y. Zahran, Correlation between the static refractive index and the optical bandgap: Review and new empirical approach, *Physica B* **620** (2021) 413246, https://doi.org/10.1016/j.physb.2021.413246.

48. H. T. Nguyen-Truong, T.-T. Pham, N. H. Vu, D. H. Ngo, and H. M. Le, Energy-loss function for lead, *Commun. Phys.* **27** (2017) 65, http://doi.org/10.15625/0868-3166/27/1/9201.

49. M. Dresselhaus, G. Dresselhaus, S. B. Cronin, and A. G. S. Filho, Solid State Properties: From Bulk to Nano (Springer-Verlag, Germany, 2018).

50. P. Y. Yu and M. Cardona, Fundamentals of Semiconductors: Physics and Materials Properties (Springer, Berlin, 2010).